

A Prediction Model for Stationary, Short-crested Waves in Shallow Water with Ambient Currents

L.H. HOLTHUIJSEN*, N. BOOIJ and T.H.C. HERBERS**

Delft University of Technology, P.O. Box 5048, 2600 GA Delft (The Netherlands)

(Received December 21, 1987; revised and accepted July 22, 1988)

ABSTRACT

Holthuijsen, L.H., Booij, N. and Herbers, T.H.C., 1989. A prediction model for stationary, short-crested waves in shallow water with ambient currents. *Coastal Eng.*, 13: 23-54.

A numerical model for the hindcasting of waves in shallow-water (HISWA) is described and comparisons are made between observations and model results in a realistic field situation. The model is based on a Eulerian presentation of the spectral action balance of the waves rather than on the more conventional (at least in coastal engineering) Lagrangian presentation. Wave propagation is correspondingly computed on a grid rather than along rays. The model accounts for refractive propagation of short-crested waves over arbitrary bottom topography and current fields. The effects of wave growth and dissipation due to wind generation, bottom dissipation and wave breaking (in deep and shallow water) are represented as source terms in the action balance equation. The computational efficiency of the model is enhanced by two simplifications of the basic balance equation. The first one is the removal of time as an independent variable to obtain a stationary model. This is justified by the relatively short travel time of waves in coastal regions. The second simplification is the parameterization of the basic balance equation in terms of a mean frequency and a frequency-integrated action density, both as function of the spectral wave direction. The discrete spectral representation of wave directionality is thus retained. An untuned version of HISWA has been tested in a closed branch of the Rhine estuary where measurements with buoys and a wave gauge are available. In this situation, where wave breaking and short-crestedness dominate, rms-errors in the significant wave height and mean wave period are about 10 and 13% respectively of the observed values.

INTRODUCTION

Coastal engineers are regularly confronted with the task of estimating wave conditions in coastal regions or in inland waters from wave information in deeper water and local wind information. This essentially entails the computation of wave propagation in nearshore regions taking into account the effects

*To whom correspondence should be sent.

**Presently at Scripps Institution of Oceanography, La Jolla, U.S.A.

of wind, bottom and currents. In this paper we formulate a numerical wave model (called HISWA = HIndcasting shallow WATER WAVES) to carry out such computations for short-crested waves with fairly limited computer capacity and we compare results of this model with observations in the Rhine estuary. The model is of a complexity which places it between models based on monochromatic wave-ray techniques and time-dependent discrete spectral wave models.

Refractive wave propagation in shallow water is sufficiently well described by linear wave theory in many coastal engineering situations. In conventional coastal engineering models this theory is implemented with the wave ray technique, either in a monochromatic approach (e.g. Arthur et al., 1952) or in a discrete spectral approach (e.g. Cavaleri and Malanotte Rizzoli, 1981; Brink-Kjær, 1984; Mathiesen, 1984). These models are of a Lagrangian nature in the sense that the wave development is considered while travelling with the waves along rays. However, this approach is numerically inefficient when nonlinear wave generation and dissipation is to be determined. The reason for this is that to compute such nonlinear phenomena the effects of wave propagation of different spectral components need to be integrated in the spectral domain. This is numerically costly in the wave-ray approach as the relevant information is available only on the wave rays and these are scattered over the area of interest. In an Eulerian approach of wave propagation all wave information is inherently available at the mesh-points of a regular grid. The nonlinear source terms are then readily computed. Such an Eulerian approach is common in models for ocean wave forecasting (e.g. Gelci et al., 1956; Barnett, 1968; Ewing, 1971). In fact some of these models have been extended to include finite depth effects (e.g. Golding, 1983; Janssen et al., 1984; Graber and Madsen, 1985; Young, 1988). Other Eulerian wave models have been designed specifically for shallow water (e.g. Piest, 1965; Battjes, 1968; Karlson, 1969; Chen and Wang, 1983; Sakai et al., 1983; Hirose and Sakai, 1987).

Ideally one would prefer a fully discrete spectral model accounting for all processes of generation and dissipation and wave-current interactions. However, the very high spatial resolution that is sometimes required in coastal areas would demand excessive computer requirements (e.g. 100×100 grid-points in an area of 10×10 km for a coastal model as compared to 35×35 gridpoints in an area of 3500×3500 km for an ocean model). Some degree of simplification is therefore needed. One simplification would be to ignore the wave-current interactions. In fact, these interactions are absent in all but one of the above Eulerian models. The exception is the model of Chen and Wang (1983) in which wave-current interactions are accounted for but in which the waves are assumed to be unidirectional at every frequency. We feel that this is unrealistic in many situations, for example when wind waves propagate through strong tidal currents or over very shallow shoals.

We introduce two simplifications to reduce the required computer capacity

to manageable proportions. The first one is based on the fact that in coastal situations the travel time of the waves through the area of interest is often short compared to the time scale of the local windfield or the ambient currents. The situation can then be treated as stationary. This simplifies the wave model considerably since it permits the removal of time as an independent variable. The second simplification is to parameterize the balance equation of wave action in the following manner. The action balance equation consists basically of three terms: the local rate of change of the spectral action density (which we removed to make the model stationary); the propagation term (including refraction and shoaling); and the source function which represents the generation and dissipation of wave action due to wind, wave breaking, etc. A full numerical treatment of the source function is not only prohibitively expensive because of the complex nature of nonlinear wave-wave interactions (e.g. Hasselmann and Hasselmann, 1981) but in fact not well possible since the source functions are not well understood in shallow water in the presence of currents. For practical applications some degree of parameterization is therefore needed. Such parameterization can be applied either to the source function alone (notably the nonlinear wave-wave interactions; e.g. Hasselmann et al., 1985) or to the spectral balance equation as a whole (e.g. Günther et al., 1979). The first option, a parameterization of the source function alone is usually sufficient for ocean wave models. However, it is not sufficient for our model as the expected number of gridpoints is potentially one order of magnitude larger than in an ocean wave model. We have therefore chosen for the second option: to parameterize the complete action balance equation. In some presently operating ocean wave models such parameterization is carried out by expressing the wave spectrum and the energy balance equation (action is not used in these models) in terms of a small number of characteristic parameters such as the significant wave height, the mean wave period and a main wave direction (e.g. Günther et al., 1979; Janssen et al., 1984). This implies a considerable reduction of frequency and directional information of the wave field. We feel that for applications in coastal waters such a parameterization is too drastic. In particular the directional details of the wave spectrum should be retained in coastal regions with a complex bathymetry where the occurrence of cross-seas is an essential aspect of the wave field. Therefore, instead of defining integral parameters such as a significant wave height, we define two directional wave functions: the directional action spectrum $A_0(\theta)$ and a mean wave frequency as a function of spectral direction $\omega_0(\theta)$. We accordingly parameterize the propagation terms and the source terms of the spectral action balance equation (the local rate of change has already been removed as indicated). The number of degrees of freedom of the wave model is thus reduced from about 125 per spatial grid point (the number of wave components in a two-dimensional spectrum) to about 25 (the number of directions of A_0 and ω_0) while retaining the

spectral representation of the directionality of the waves. To implement the HISWA model on a computer we have used a finite difference method.

The model has been applied to waves penetrating a closed branch of the Rhine estuary where detailed wave observations are available (Dingemans, 1983; Dingemans et al., 1985) using a priori chosen coefficients from the literature. Experimental computations show that the observed situation is dominated by wave breaking and short-crestedness, suppressing the effects of refraction. Such combination is usually not handled well by other models. We found the rms-error of the model results to be 10.2 and 13.0% respectively of the observed values of the significant wave height (which varied from about 3.0 to about 0.5 m) and of the mean wave period (which varied from about 7.0 to about 2.5 s).

PHYSICAL BACKGROUND

Introduction

Models for hindcasting waves in the absence of currents are usually based on the energy balance equation of the waves in which the wave energy density E , as a function of absolute frequency ω and direction θ , is considered as a slowly varying function in space (x,y) and time t (e.g. Gelci et al., 1956; Hasselmann, 1960; Phillips, 1977). However, in the presence of an ambient current the more relevant wave parameter for modelling purposes is action density A defined as (e.g. Whitham, 1965, 1971):

$$A(\omega, \theta; x, y, t) = E(\omega, \theta; x, y, t) / \sigma \quad (1)$$

with the relative frequency σ defined as:

$$\sigma = \omega - \mathbf{k} \cdot \mathbf{V} \quad (2)$$

in which \mathbf{k} is the wavenumber vector (magnitude k and direction θ) and \mathbf{V} is the current velocity vector. The action balance equation, which replaces the more conventional energy balance equation, is then, in the adopted Eulerian approach (dropping the notation for the independent variables from A):

$$\frac{\partial A}{\partial t} + \frac{\partial}{\partial x}(c_x A) + \frac{\partial}{\partial y}(c_y A) + \frac{\partial}{\partial \theta}(c_\theta A) + \frac{\partial}{\partial \omega}(c_\omega A) = T \quad (3)$$

The local rate of change of action density is represented by the first term on the left-hand side of Eq. 3. The other terms on the left-hand side represent the net transport of action in the x -, y -, θ -, and ω -domain respectively. The total effect of generation and dissipation of action (e.g. by wind) is represented by the action source function T . It is also a function of x , y , t , θ and ω .

The propagation speeds c_x and c_y in the balance equation (Eq. 3) are defined

as the x - and y -component respectively of the action propagation speed in (x,y) -space, also called the group velocity \mathbf{c} . In linear wave theory \mathbf{c} is defined as:

$$\mathbf{c} = \frac{\partial \sigma}{\partial \mathbf{k}} + \mathbf{V} \quad (4)$$

It should be noted that in the presence of a current the direction of the group velocity \mathbf{c} is in general not equal to the wave direction θ (the direction normal to the wave crest of wave component (θ, ω)).

The propagation speed c_θ , representing refraction (see below), is given by linear wave theory as:

$$c_\theta = -\frac{1}{k} \frac{\partial \sigma}{\partial d} \frac{\partial d}{\partial n} - \frac{\mathbf{k}}{k} \cdot \frac{\partial \mathbf{V}}{\partial n} \quad (5)$$

in which d is the local water depth and n is the coordinate in (x,y) -space normal to the spectral wave direction θ .

The propagation speed c_ω , which represents the shift of action in the frequency domain induced by time variations in the propagation medium (variations in water depth or current speed and direction) is given by:

$$c_\omega = \mathbf{k} \cdot \frac{\partial \mathbf{V}}{\partial t} + \frac{\partial \sigma}{\partial d} \frac{\partial d}{\partial t} \quad (6)$$

This representation of wave propagation in the action balance equation (Eq. 3) is unconventional in coastal engineering. The more usual representation is based on wave ray techniques. Fundamentally there is no difference as both approaches represent wave propagation according to the linear theory of surface gravity waves. However, some explanation of the correspondence between the two approaches seems in order. To do this, we consider a situation where the wave field, the bottom topography and the current fields are constant in time. In such a situation the first and fifth term on the left-hand side of the action balance equation (Eq. 3) vanish. This is a situation normally considered when using the wave ray approach. When following the wave energy along a wave ray, the energy is followed across x,y -space with the group velocity with x - and y -component c_x and c_y respectively (the difference between energy and action is not essential for this explanation). This illustrates that the second and third term on the left hand side represent propagation in x,y -space at a given location x,y in a given direction θ . However, in general the direction of the energy propagation is not a constant as wave rays in shallow water are usually not straight lines due to refraction. A curving wave ray implies that the direction of wave propagation changes while travelling along the ray. In other words the energy continually changes direction while travelling through x,y -space. This can be conceived as the energy travelling not only through x,y -space but also (and simultaneously) through θ -space. The travel speed in θ -

space is the rate at which the direction changes as one travels with the group velocity along the (curving) ray. This rate of change is the above speed c_θ . This illustrates that the fourth term on the left hand side represents refraction. The effect of currents is taken into account by including the current speed and direction in the expressions for c_x , c_y , and c_θ and by using action density rather than energy density in the formulation (Bretherton and Garrett, 1968).

For the HISWA model we consider precisely such stationary situations as indicated above. The basic equation of our model therefore reduces to:

$$\frac{\partial}{\partial x}(c_x A) + \frac{\partial}{\partial y}(c_y A) + \frac{\partial}{\partial \theta}(c_\theta A) = T \quad (7)$$

with c_x , c_y and c_θ as given above.

However, as indicated in the introduction, this equation is still too complex for a full numerical treatment. We therefore parameterize this equation as a whole with the side-condition that the directional characteristics of the waves should be retained. To this end we have chosen the zero-th and first-order moments of the action spectrum in the frequency domain for the parameterization. The corresponding two wave functions are the one-dimensional directional action spectrum $A_0(\theta)$ and the mean frequency as a function of spectral direction $\omega_0(\theta)$:

$$A_0(\theta) = m_0(\theta) \quad (8)$$

$$\omega_0(\theta) = m_1(\theta)/m_0(\theta) \quad (9)$$

in which the moments m_n of the action density spectrum are defined as:

$$m_n(\theta) = \int_0^\infty \omega^n A(\omega, \theta) d\omega \quad (10)$$

Note that the function $A_0(\theta)$ is a directional spectrum in the sense that it presents the directional distribution of frequency-integrated wave action density. It is not the directional spectrum in the more conventional sense of a two-dimensional wave spectrum, e.g. $A(\omega, \theta)$. The parameterization of the action balance equation is carried out by applying the definition operator used in Eq. 10 with $n=0$ and $n=1$ to the basic balance equation (Eq. 7). This gives two evolution equations: one for $m_0(\theta)$ and one for $m_1(\theta)$. The corresponding equations are (dropping θ from the notation):

$$\frac{\partial}{\partial x}(c_{0x}^* m_0) + \frac{\partial}{\partial y}(c_{0y}^* m_0) + \frac{\partial}{\partial \theta}(c_{0\theta}^* m_0) = T_0 \quad (11)$$

$$\frac{\partial}{\partial x}(c_{1x}^{**} m_1) + \frac{\partial}{\partial y}(c_{1y}^{**} m_1) + \frac{\partial}{\partial \theta}(c_{1\theta}^{**} m_1) = T_1 \quad (12)$$

in which c_{0x}^* , c_{0y}^* and $c_{0\theta}^*$ in Eq. 11 and c_{0x}^{**} , c_{0y}^{**} and $c_{0\theta}^{**}$ in Eq. 12 are the propagation speeds through (x,y,θ) -space of m_0 and m_1 respectively. T_0 and T_1 are the parameterized source functions for m_0 and m_1 respectively. Equations 11 and 12 are implemented in the HISWA model.

The propagation part of these equations (left-hand side) and the generation/dissipation part (right-hand side) are addressed next.

Propagation

In view of other uncertainties in our model (particularly the generation and dissipation of waves in shallow water), the propagation speeds in Eq. 11 and 12 are taken equal to the corresponding speeds at the mean frequency ω_0 ; c_{0x} , c_{0y} and $c_{0\theta}$. Of these, c_{0x} and c_{0y} are the x - and y -component respectively of the group velocity \mathbf{c}_0 at frequency ω_0 (see Eq. 4):

$$\mathbf{c}_0 = \frac{\partial \sigma_0}{\partial \mathbf{k}_0} \frac{\mathbf{k}_0}{k_0} + \mathbf{V} \quad (13)$$

in which \mathbf{k}_0 is the wavenumber vector corresponding to $\omega_0(\theta)$ (with magnitude k_0 and direction θ) determined from linear wave theory by:

$$\omega_0 = \sigma_0 + \mathbf{k}_0 \cdot \mathbf{V} \quad (14)$$

and:

$$\sigma_0 = \{gk_0 \tanh(k_0 d)\}^{1/2} \quad (15)$$

The propagation speed representing refraction at the mean frequency ω_0 , $c_{0\theta}$ is, from linear wave theory:

$$c_{0\theta} = -\frac{1}{k_0} \frac{\partial \sigma_0}{\partial d} \frac{\partial d}{\partial n} - \frac{\mathbf{k}_0}{k_0} \cdot \frac{\partial \mathbf{V}}{\partial n} \quad (16)$$

The source functions T_0 and T_1 are derived below using the above assumptions regarding the propagation speeds.

Generation and dissipation

Formally the source functions T_0 and T_1 can be obtained by parameterizing the action source function T of Eq. 3. However, this function is only partially known and rather complex. Therefore, instead of attempting such a formal parameterization we express T_0 and T_1 in terms of functions which can be estimated more readily, at least to some extent, from information in the literature. To this end we express T_0 and T_1 in terms of the source functions of wave energy (S_E) and the mean frequency of the energy spectrum (S_ω).

If the directional action density $A_0(\theta)$ is approximated by the frequency integrated directional energy density $E_0(\theta)$ ($= \int_0^\infty E(\omega, \theta) d\omega$) divided by $\sigma_0(\theta)$ then the source function of $m_1(\theta)$, T_1 is the rate at which $E_0\omega_0/\sigma_0$ is generated or dissipated. If we assume that the frequencies ω_0 and σ_0 are approximately equally affected by wave generation and dissipation so that their ratio varies only slowly, then T_1 is related in a simple fashion to S_E , the rate at which $E_0(\theta)$ is generated or dissipated:

$$T_1 \cong \frac{\omega_0}{\sigma_0} S_E \quad (17)$$

S_E will be determined below from information in the literature.

The source function for m_0 , T_0 can be readily formulated in terms of S_E and S_ω , the rate of change of the mean frequency $\omega_0(\theta)$. This is achieved by first subtracting Eq. 11 multiplied by ω_0 from Eq. 12. The result of this is:

$$c_{0x} \frac{\partial \omega_0}{\partial x} + c_{0y} \frac{\partial \omega_0}{\partial y} + c_{0\theta} \frac{\partial \omega_0}{\partial \theta} = \frac{1}{A_0} (T_1 - \omega_0 T_0) \quad (18)$$

of which the left-hand side represents the evolution of ω_0 in stationary conditions ($= S_\omega$). Substituting T_1 from Eq. 17 in Eq. 18, the source function T_0 can be obtained in terms of S_E and S_ω as:

$$T_0 \cong \frac{1}{\sigma_0} S_E - \frac{A_0}{\omega_0} S_\omega \quad (19)$$

The source functions $S_E(\theta)$ and $S_\omega(\theta)$ represent the effects of generation and dissipation. We therefore write them as the sum of their constituent source terms:

$$S_E(\theta) = S_E(\theta)_{\text{wind}} + S_E(\theta)_{\text{bottom}} + S_E(\theta)_{\text{breaking}} + S_E(\theta)_{\text{blocking}} \quad (20)$$

$$S_\omega(\theta) = S_\omega(\theta)_{\text{wind}} + S_\omega(\theta)_{\text{bottom}} + S_\omega(\theta)_{\text{breaking}} + S_\omega(\theta)_{\text{blocking}} \quad (21)$$

The subscripts wind, bottom, breaking and blocking refer to wind generation, bottom friction, wave breaking and current-induced blocking of wave propagation respectively. In the following we formulate these source terms in a fairly pragmatic way. The reasons for this are firstly, that we wish to use rather simple expressions to avoid costly computations and secondly, that detailed information on each of the individual source terms is not available for very shallow water (e.g. the effects of shallow-water wave breaking). In addition the formulations are such that the results of rather basic numerical or physical experiments can be readily incorporated in the model. It should be noted that wind generation is interpreted in the present context to include all processes of wave generation and dissipation in deep water (i.e. wind input, nonlinear

wave-wave interactions and deep-water wave breaking in the absence of currents).

Instead of addressing the source function of the action-averaged frequency $S_\omega(\theta)$ we will address in the following the source function $S_\Omega(\theta)$ of the energy-averaged frequency $\Omega_0(\theta)$:

$$\Omega_0(\theta) = \frac{1}{E_0(\theta)} \int_0^\infty \omega E(\omega, \theta) d\omega \quad (22)$$

The reason for this change from $\omega_0(\theta)$ to $\Omega_0(\theta)$ is that information on the energy-averaged frequency $\Omega_0(\theta)$ is more readily available in the literature than on the action-averaged frequency $\omega_0(\theta)$. The ratio of the values of $\omega_0(\theta)$ and $\Omega_0(\theta)$ is usually close to one, in fact, in HISWA we use the value for the mean JONSWAP spectrum ($\omega_0/\Omega_0=0.92$; Hasselmann et al., 1973). We correspondingly take $S_\omega = \omega_0/\Omega_0 S_\Omega$.

To roughly estimate the nature and the magnitude of the source terms we assume in the following a shape of the wave spectrum without implying that the model predicts such a shape. Other assumptions on the spectral shape would probably give roughly the same results. Of course, it would be a simple matter to supplement the output of the model with a standard shape frequency spectrum for each spectral direction (with $E_0(\theta)$ and $\Omega_0(\theta)$ as parameters, e.g. the k^{-3} -spectrum of Eq. 39 or a JONSWAP spectrum (Hasselmann et al., 1973) modified with the Kitaigorodskii scaling, e.g. Bouws et al., 1985).

Generation by wind

The formulation of wave generation by wind is taken from empirical information in an idealized situation. This situation is one in which a stationary, spatially uniform wind with velocity U starts to blow over deep water (no currents, no waves) at time $t=0$. In such a situation, we formulate the evolution in time of the total wave energy E_1 and the overall mean frequency Ω_1 as:

$$E_1 = \int_0^{2\pi} E_0(\theta) d\theta \quad (23)$$

and:

$$\Omega_1 = \frac{1}{E_1} \int_0^{2\pi} \Omega_0(\theta) E_0(\theta) d\theta \quad (24)$$

with the following expressions:

$$\left. \begin{aligned} \tilde{E}_1 &= a \tilde{t}^b & \text{for } \tilde{t} < \tilde{t}_m \\ \tilde{E}_1 &= a \tilde{t}_m^b & \text{for } \tilde{t} \geq \tilde{t}_m \end{aligned} \right\} \quad (25)$$

and:

$$\left. \begin{aligned} \tilde{\Omega}_1 &= c \tilde{t}^d & \text{for } \tilde{t} < \tilde{t}_m \\ \tilde{\Omega}_1 &= c \tilde{t}_m^d & \text{for } \tilde{t} \geq \tilde{t}_m \end{aligned} \right\} \quad (26)$$

in which \tilde{E}_1 , $\tilde{\Omega}_1$ and \tilde{t} are dimensionless representations of E_1 , Ω_1 and t based on wind speed U and gravitational acceleration g . Taking the time derivative of Eq. 25 and 26 gives expressions for $S_E(\theta)$ and $S_\Omega(\theta)$ in terms of dimensionless time \tilde{t} provided that we assume the normalized directional energy distribution $D(\theta)$ in this ideal case to be constant in time, so that:

$$E_0(\theta) = E_1 D_{\text{ideal}}(\theta) \quad (27)$$

and that $\Omega_0(\theta)$ is constant over θ , so that:

$$\Omega_0(\theta) = \Omega_1 \quad (28)$$

To determine $S_E(\theta)$ and $S_\Omega(\theta)$ we use a directionally decoupled parametric model the notion of which has been suggested by Seymour (1977). It is based on the assumption that the two-dimensional energy density in direction θ develops independently from the energy densities in other directions (but it does depend on the energy density at other frequencies in the same direction). The validity of these suggestions is supported by Holthuijsen (1983) who observed directional wave spectra with a high directional resolution which in off-shore wind conditions were affected by the shape of the up-wind coast. The observed effects could be reconstructed with a directionally decoupled parametric model. Observations with similar characteristics were obtained by Donelan et al. (1985). $S_E(\theta)$ and $S_\Omega(\theta)$ are correspondingly taken to be dependent on the equivalent total wave energy $E_1^*(\theta) = E_0(\theta)/D_{\text{ideal}}$ and the equivalent mean wave frequency $\Omega_1^*(\theta) = \Omega_0(\theta)$. During the computations $E_1^*(\theta)$ and $\Omega_1^*(\theta)$ are substituted in Eq. 25 and 26 to obtain equivalent dimensionless durations $\tilde{t}(\theta)$ for $E_1^*(\theta)$ and $\Omega_1^*(\theta)$ respectively which in turn provide the rates of change of $E_1^*(\theta)$ and $\Omega_1^*(\theta)$. The rate of change of $E_1^*(\theta)$ is directionally distributed with D_{ideal} to find $S_E(\theta)$. In HISWA we take $D_{\text{ideal}} = A \cos^n(\theta - \theta_w)$ in which θ_w is the wind direction and n is usually taken 2.0. $S_\Omega(\theta)$ is found by assuming the rate of change of $\Omega_1^*(\theta)$ to be independent of θ . The values of $S_E(\theta)$ and $S_\Omega(\theta)$ are thus determined solely from the values of $E_0(\theta)$ and $\Omega_0(\theta)$ and the wind speed and direction. To obtain results of deep-water wave growth comparable with those of the Shore Protection Manual (CERC, 1973) in another ideal situation (where a constant wind blows perpendicular off a long and straight coast with no currents), we choose the values of the constants in Eq. 25 and 26 as: $a = 1.44 \times 10^{-8}$; $b = 1.12$; $c = 43.59$; $d = -1/3$; and $\tilde{t}_m = 6.6 \times 10^4$ (see Fig. 1).

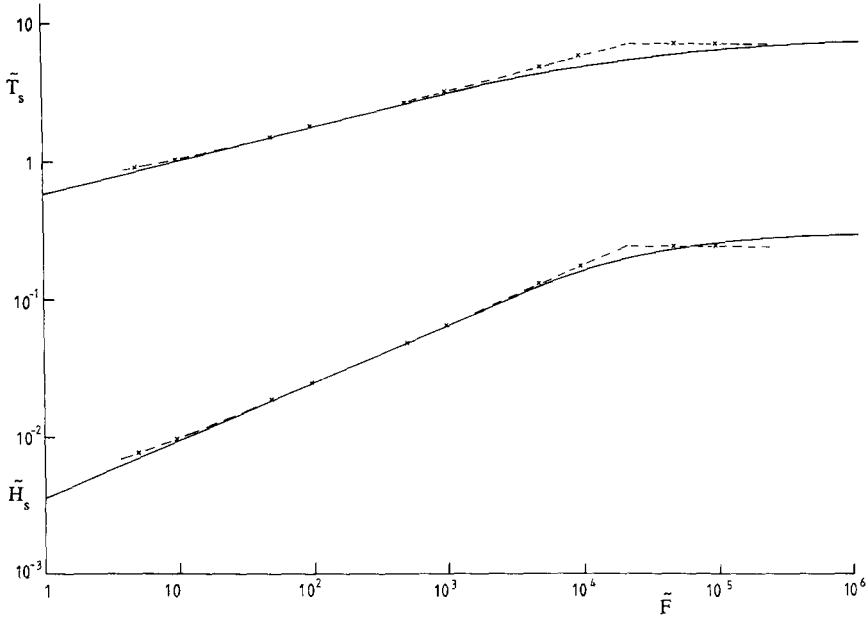


Fig. 1. Growth curves for fetch-limited conditions according to Shore Protection Manual (CERC, 1973, full lines) and HISWA (crosses and dashed lines). Dimensionless significant wave height (\tilde{H}_s); wave period (\tilde{T}_s ; $\tilde{T}_s = 1.2 \bar{T}$ assumed); and fetch (\tilde{F}) on basis of wind speed (U) and gravitational acceleration (g).

For the evolution of $\Omega_0(\theta)$ in non-ideal situations, we assume that the wind generation forces the value of $\Omega_0(\theta)$ towards the following directional equivalent of the universal relationship $\tilde{\Omega}_1 = e \tilde{E}_1^f$ (e.g. Hasselmann et al., 1976):

$$\tilde{\Omega}_0(\theta) = e \{ \tilde{E}_0(\theta) / D_{\text{ideal}}(\theta) \}^f \quad (29)$$

in which \tilde{E}_1 , $\tilde{E}_0(\theta)$, $\tilde{\Omega}_1$ and $\tilde{\Omega}_0$ are dimensionless representations of E_1 , $E_0(\theta)$, Ω_1 and $\Omega_0(\theta)$ based on wind speed U and gravitational acceleration g . It follows from Eq. 25 and 26 that $e = ca^{-d/b}$ and $f = d/b$. To achieve this behaviour of the model we have chosen the following relaxation formulation:

$$S_{\Omega}(\theta)_{\text{wind}} = S_{\Omega, \text{ideal}}(\theta)_{\text{wind}} \left(\frac{\tilde{\Omega}_0(\theta)}{e \{ \tilde{E}_0(\theta) / D_{\text{ideal}}(\theta) \}^f} \right)^m \quad (30)$$

thus forcing the value of $\Omega_0(\theta)$ towards the value imposed by Eq. 29. The value of m , governing the rate of relaxation, has been chosen such ($m=5$) that the model results are similar to those obtained by Günther (1981) (see Fig. 2). This illustration shows the evolution of \tilde{E}_1 and $\tilde{\Omega}_1$ in a homogeneous, stationary wind field for various initial values of \tilde{E}_1 and $\tilde{\Omega}_1$.

The effect of currents on wave generation is accounted for in the model by taking the wind speed and direction relative to the current.

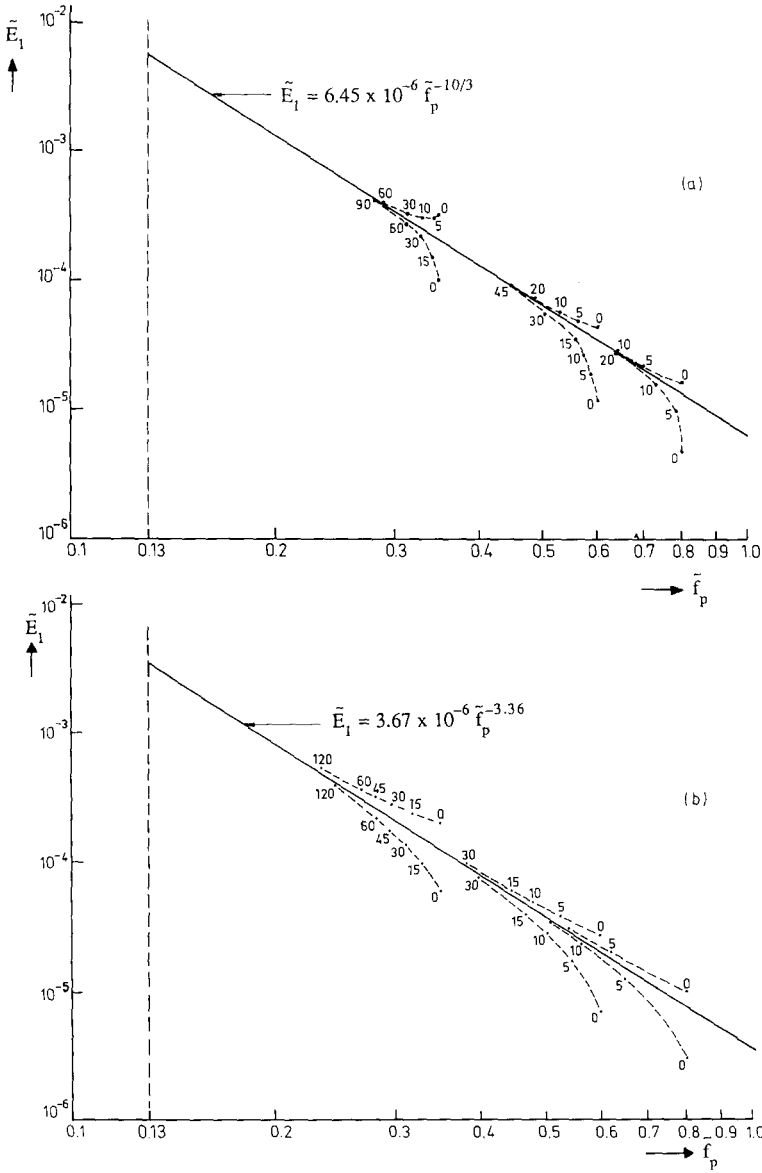


Fig. 2. Relaxation of the dimensionless wave energy (\tilde{E}_1) and the dimensionless peak frequency (\tilde{f}_p ; $\Omega_1 = 0.75 \, 2\pi f_p$ assumed) to the universal relationship (full lines); according to Günther (1981, panel a) and HISWA (panel b); time in min.

Bottom dissipation

Bottom dissipation in our model is based on the conventional quadratic friction law to represent bottom shear stress. The corresponding energy dissipa-

tion for a harmonic wave with frequency ω and energy $E_1 = \frac{1}{8}H^2$ is (e.g. Putnam and Johnson, 1949):

$$\left(\frac{dE_1}{dt}\right)_{\text{bottom}} = \frac{-1}{6\pi} \frac{c_{fw}}{g} \left(\frac{\omega H}{\sinh(kd)}\right)^3 \quad (31)$$

in which c_{fw} is a friction coefficient and H is the wave height. Note that energy is interpreted here and anywhere else in this paper as variance. This expression has been extended by Dingemans (1983) to unidirectional random waves with Rayleigh distributed wave heights, (one single frequency ω):

$$\left(\frac{dE_1}{dt}\right)_{\text{bottom}} = \frac{-1}{8\pi^{1/2}} \frac{c_{fw}}{g} \frac{\omega^3}{\sinh^3(kd)} H_{\text{rms}}^3 \quad (32)$$

in which H_{rms} is the rms-value of the wave height ($H_{\text{rms}} = 2(2E_1)^{1/2}$ if the waves are Rayleigh distributed). Ignoring the negative sign for the moment, this expression may be written as the product of a measure $\langle \tau \rangle$ of the shear-stress proportional to the orbital velocity squared and a measure $\langle v \rangle$ of the orbital velocity at the bottom:

$$\langle \tau \rangle = (8/\pi)^{1/2} \frac{c_{fw}}{g} \frac{\omega^2}{\sinh^2(kd)} E_1 \quad (33)$$

$$\langle v \rangle = \frac{\omega}{\sinh(kd)} E_1^{1/2} \quad (34)$$

To obtain a simple directional version of this formulation we assume, analogous to the above, that the shear stress is directionally distributed in proportion to the square of the orbital velocity in each direction:

$$\langle \tau(\theta) \rangle = (8/\pi)^{1/2} \frac{c_{fw}}{g} \frac{\Omega_0^2(\theta)}{\sinh^2\{k_0(\theta)d\}} E_0(\theta) \quad (35)$$

In view of the nonlinear character of the bottom dissipation we assume that the dissipation in each direction is coupled to the other directions through the magnitude of the orbital velocity at the bottom (estimated analogous to Collins, 1972):

$$\langle v_1 \rangle = \left[\int_0^{2\pi} \frac{\Omega_0^2(\theta) E_0(\theta)}{\sinh^2\{k_0(\theta)d\}} d\theta \right]^{1/2} \quad (36)$$

We consequently write the directional distribution of the bottom dissipation as:

$$S_E(\theta)_{\text{bottom}} = - \langle \tau(\theta) \rangle \langle v_1 \rangle \quad (37)$$

The effect of a mean current on the bottom dissipation is taken into account

by adding the current component in the θ -direction, V_θ to the characteristic orbital velocity $\langle v_1 \rangle$, with its own friction coefficient c_{fc} , and by replacing the absolute frequency $\Omega_0(\theta)$ by the relative frequency $\sigma_0(\theta)$ in the source term $S_E(\theta)_{\text{bottom}}$ (Eq. 35, 36 and 37):

$$S_E(\theta)_{\text{bottom}} = - (8/\pi)^{1/2} \frac{(c_{fw} \langle v_1 \rangle + c_{fc} V_\theta)}{g} \frac{\sigma_0^2(\theta)}{\sinh^2\{k_0(\theta)d\}} E_0(\theta) \quad (38)$$

in which $V_\theta = V_x \cos \theta + V_y \sin \theta$.

To formulate the effect of bottom dissipation on the mean frequency $\Omega_0(\theta)$ we assume that this dissipation is concentrated at the low frequency side of the wave spectrum because the longest waves are more affected by the bottom than the shorter waves. In addition, the spectrum is assumed to have a universal high-frequency tail if expressed in terms of wavenumber k , in both deep and shallow water (e.g. Kitaigorodskii et al., 1975; Thornton, 1977). Our directional version of this universal spectrum is:

$$\left. \begin{aligned} E(k, \theta) &= \alpha(\theta) k^{-n} & \text{for } k \geq k_p \\ E(k, \theta) &= 0 & \text{for } k < k_p \end{aligned} \right\} \quad (39)$$

in which k_p is the peak wave number and $n=3$ (Kitaigorodskii et al., 1975; Thornton, 1977). The rate of change of the mean frequency $\Omega_0(\theta)$ as induced by this low-frequency bottom dissipation is estimated by first considering the corresponding rate of change of the mean wavenumber $K_0(\theta)$ defined as:

$$K_0(\theta) = \frac{1}{E_0(\theta)} \int_0^\infty k E(k, \theta) dk \quad (40)$$

It is readily shown that for the assumed spectrum of Eq. 39 with $\alpha(\theta)$ constant in time, the rate of change of $K_0(\theta)$ is directly related to $S_E(\theta)_{\text{bottom}}$ as:

$$\frac{d}{dt}(K_0(\theta)) = \frac{1}{(1-n)} \frac{K_0(\theta)}{E_0(\theta)} S_E(\theta)_{\text{bottom}} \quad (41)$$

If we replace ω_0 and k_0 by $\Omega_0(\theta)$ and $K_0(\theta)$ in Eq. 14 and 15, assuming that these equations hold for $\Omega_0(\theta)$ and $K_0(\theta)$, the rate of change of $\Omega_0(\theta)$ is readily determined from Eq. 41:

$$S_{\Omega}(\theta)_{\text{bottom}} = \frac{1}{(1-n)} \frac{c_0(\theta) K_0(\theta)}{E_0(\theta)} S_E(\theta)_{\text{bottom}} \quad (42)$$

The effect of a current on the mean frequency is implicit in the formulation of $S_{\Omega}(\theta)_{\text{bottom}}$ through $S_E(\theta)_{\text{bottom}}$ in Eq. 42, and in the propagation speed $c_0(\theta)$ and the determination of $K_0(\theta)$ from $\Omega_0(\theta)$ with Eq. 14 and 15.

Wave breaking

To account for wave breaking due to a large wave steepness or due to direct bottom effects (e.g. over shoals or on a beach), to the extent that it has not been accounted for implicitly in $S_E(\theta)_{\text{wind}}$ and $S_\Omega(\theta)_{\text{wind}}$, we use the expression of Battjes and Janssen (1979) in our notation:

$$\left(\frac{dE_1}{dt}\right)_{\text{breaking}} = -\alpha_1 Q_b \Omega_1 H_m^2 / (8 \pi) \quad (43)$$

in which H_m is a maximum wave height, Q_b is the fraction of breaking waves (estimated from the Rayleigh distribution for wave heights and the value of H_m (Battjes and Janssen, 1979) and α_1 is a numerical constant. The value of H_m is taken by Battjes and Janssen (1979) from the criteria of Miche (1944) (wave steepness in deep water and water depth in shallow water):

$$H_m = \gamma_1 k_1^{-1} \tanh(\gamma_2 k_1 d / \gamma_1) \quad (44)$$

with k_1 obtained from Ω_1 with the linear wave theory. We choose the directional distribution of this dissipation such that it does not influence the shape of the directional energy distribution:

$$S_E(\theta)_{\text{breaking}} = -\alpha_1 Q_b \Omega_0(\theta) H_m^2 E_0(\theta) / (8 \pi E_1) \quad (45)$$

We have considered to use the values of α_1 , γ_1 and γ_2 as used by Battjes and Janssen (1979) (viz. 1.0, 0.88 and 0.8 respectively) but since in our model some deep water breaking is already implicitly accounted for in the wind generation terms, we wished to trigger the above dissipation term at higher values for wave steepness (controlled by γ_1). After some trial and error we choose $\gamma_1 = 1.0$ (wave steepness $H_m/L_1 = 0.16$; where L_1 is $2\pi/k_1$) as a fairly low value (i.e. close to 0.88 or $H_m/L_1 = 0.14$) for which the dissipation modelled by Eq. 45 does not affect deep water wave growth significantly. The values of α_1 and γ_2 in the HISWA model are those used by Battjes and Janssen (1979).

The effect of the above wave breaking mechanism on the mean frequency in shallow water is chosen to be similar to the effect of bottom dissipation (low-frequency dissipation) since in the above model of Battjes and Janssen (1979) only the highest waves (with lowest frequencies) break. We assume that in deep water the mean frequency is not influenced by wave breaking. This behaviour of the model is achieved by using an expression for $S_\Omega(\theta)_{\text{breaking}}$ similar to that of $S_\Omega(\theta)_{\text{bottom}}$ multiplied with a depth dependent reduction factor R the value of which is 0 in deep water and 1 in shallow water:

$$S_\Omega(\theta)_{\text{breaking}} = \frac{R}{1-n} \frac{c_0(\theta) K_0(\theta)}{E_0(\theta)} S_E(\theta)_{\text{breaking}} \quad (46)$$

in which R is:

$$R = 1 - \{ \tanh(\gamma_2 k_1 d) \}^2 \quad (47)$$

The effect of currents on wave breaking is included in the above source terms to the extent that the propagation speed $c_0(\theta)$ is influenced by the current and to the extent that $K_0(\theta)$ is determined with Eq. 14 and 15.

Wave blocking

In a situation with a strong opposing current some fraction of the wave energy cannot be transported upstream because the group velocity of the highest frequencies in the spectrum is less than the opposing current velocity. This fraction of the wave energy may be dissipated or reflected by the counter current. The lowest frequency above which this phenomenon of wave blocking occurs (the critical frequency ω_c) is the maximum frequency for which a solution exists for the wavenumber k in the dispersion relationship:

$$\omega_c - \mathbf{k} \cdot \mathbf{U} - [gk \tanh(kd)]^{1/2} = 0 \quad (48)$$

The corresponding wavenumber is the critical wavenumber k_c . To estimate the rates of change of $E_0(\theta)$ and $\Omega_0(\theta)$ induced by wave blocking we again assume that the shape of the wavenumber spectrum is a k^{-n} -tail, (see Eq. 39), except that in this wave blocking situation no wave energy is present above the critical wavenumber:

$$\left. \begin{aligned} E(k, \theta) &= \alpha(\theta) k^{-n} && \text{for } k_p < k < k_c \\ E(k, \theta) &= 0 && \text{for } k < k_p \text{ or } k > k_c \end{aligned} \right\} \quad (49)$$

The rate of energy dissipation for this spectrum (with $\alpha(\theta)$ constant in time) is directly related to the current induced rate of change of the critical wavenumber. It follows directly from the time derivative of $E_0(\theta)$ corresponding to Eq. 49 that:

$$S_E(\theta)_{\text{blocking}} = \frac{k_c^{-n} (1-n)}{(k_c^{1-n} - k_p^{1-n})} E_0(\theta) \frac{dk_c(\theta)}{dt} \quad (50)$$

where $dk_c(\theta)/dt$ is the current induced rate of change of k_c determined in the model with Eq. 48. The corresponding rate of change of the mean wavenumber $K_0(\theta)$ follows directly from the rate of change of $k_c(\theta)$:

$$\frac{d}{dt} (K_0(\theta)) = \{k_c(\theta) - K_0(\theta)\} S_E(\theta)_{\text{blocking}} / E_0(\theta) \quad (51)$$

Replacing ω_0 and k_0 by $\Omega_0(\theta)$ and $K_0(\theta)$ in Eq. 14 and 15, and assuming that the equations hold for $\Omega_0(\theta)$ and $K_0(\theta)$, the rate of change of $\Omega_0(\theta)$ is readily determined from Eq. 51:

$$S_\Omega(\theta)_{\text{blocking}} = c_0(\theta) \{k_c(\theta) - K_0(\theta)\} S_E(\theta)_{\text{blocking}} / E_0(\theta) \quad (52)$$

The primary effect of the above formulation of blocking is to decrease the mean frequency of the waves $\Omega_0(\theta)$ to a value that is sufficiently low to permit the waves to propagate against the current. The secondary effect is to change the main wave direction of the waves ($\bar{\theta}$, see paragraph on input/output) away from opposing the direction of the current because the more the propagation direction opposes the current direction, the stronger the blocking effect will be. The mean current therefore affects the shape of the directional energy distribution.

Note

It should be noted that the effects of currents on the evolution of the waves in the propagation area are not limited to the above indicated effects on the source terms. The currents also influence the propagation, and therefore the residence time of the waves in the area of interest. The integrated effects of wind generation, bottom dissipation and wave breaking are thus indirectly influenced. Currents also cause a type of shoaling effect which may either increase or decrease the wave energy (which in turn may affect wave breaking).

NUMERICAL BACKGROUND

Numerical method

The evolution equations for $A_0(\theta)$ and for the product $\omega_0(\theta)A_0(\theta)$, Eq. 11 and 12, are partial differential equations of first order with the horizontal coordinates x and y and the spectral direction θ as independent variables. Due to the nature of the equation the state in a point in (x,y,θ) -space (e.g. the value of A_0) is determined by the state upwave from this point (upwave as defined by the propagation speeds c_{0x} , c_{0y} and the directional rate of change $c_{0\theta}$). We have therefore chosen to carry out the computation in a direction roughly parallel to the main wave propagation direction (x -direction in Fig. 3). A consequence of this is that only waves can be represented in the model which make an angle of less than 90° with the computational direction. The computation is carried out using a leap-frog finite difference scheme for propagation in (x,y) -space with user-controlled numerical diffusion added and an upstream finite difference scheme for propagation in θ -space (i.e. refraction). The leap-frog scheme is a diffusion-free second-order scheme, the upstream scheme is a first-order scheme with inherent numerical diffusion (of order $\Delta\theta$). Both schemes are subject to stability conditions, as a consequence of which the angle between wave propagation and computational direction is further restricted. It depends on the mesh sizes; typically the angle is less than 60° . The total directional sector is therefore less than 120° . This seems to be acceptable for most applications of our model since either the waves propagate from deep water to the

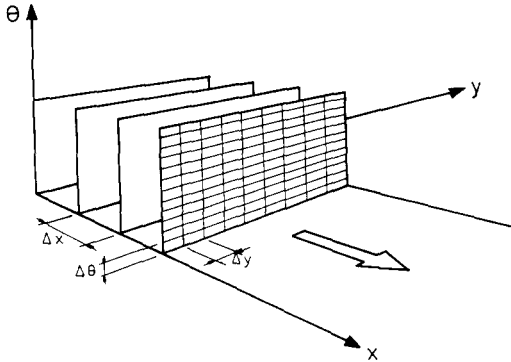


Fig. 3. Diagram of the method of stepwise computation in mean wave direction.

coast with directional changes usually less than 90° or the waves are generated by a local wind within a sector of 90° on both sides of the wind direction. However, this directional restriction implies some limitations on the use of the model. For instance, the propagation of two wave fields crossing each other at large angles is not properly modelled (e.g. locally generated wind sea orthogonal to swell). In such cases one may find an approximate solution by combining the model results obtained separately for each wave field.

Boundary conditions

The boundary conditions for the above partial differential equations are in general the specification of the wave field entering the computation area and the absorption of waves at the boundaries where the waves leave the computation area.

Since we have restricted wave directions to a sector of less than 180° and since wave information along the lateral boundaries in (x,y) -space is usually not available we assume that wave information is given only along the upwave boundary of the model in (x,y) -space (which may or may not be on land). At the other boundaries in (x,y,θ) -space we assume that no waves enter the model. One consequence of these assumptions is that energy which is refracted to outside the directional sector is removed from the model (transported across the boundaries in θ -domain where it is fully absorbed). Another consequence of the above assumptions is that the wave field near the lateral boundaries in (x,y) -space is not well represented in the model since no wave energy enters the area across these boundaries. These boundaries must therefore be chosen far enough from the area of interest. In a nested mode the model accepts wave information along the lateral boundaries in (x,y) -space that is provided by previous computations with the model.

Digitization

Two grids are used in the model: a two-dimensional grid in (x,y) -space to represent the bathymetry and the current field and a three-dimensional grid in (x,y,θ) -space to compute the wave field. Each may have different resolution and orientation in (x,y) -space as long as the wave field grid is covered by the bottom/current grid (wind is constant and therefore needs no grid). The mesh sizes Δx and Δy of the bottom/current grid should be small enough to resolve relevant spatial details in the bathymetry and in the current field. For the three-dimensional wave field grid the spatial resolutions Δx , Δy and $\Delta\theta$ should be sufficient to resolve the relevant spatial variations of the wave field, the horizontal scales of which are roughly equal to those of the bathymetry or of the current field. The value of $\Delta\theta$ depends very much on the width and the smoothness of the functions $A_0(\theta)$ and $\omega_0(\theta)$. For swell, with a narrow directional width of $A_0(\theta)$ (10° on either side of the mean wave direction, say), a relatively high resolution is required (e.g. $\Delta\theta=2^\circ$ or 3°) whereas for a typical wind sea, with a directional width of $(A_0(\theta))$ of about 30° on either side of the wind direction, a directional resolution of about 10° seems to be sufficient. To resolve spatial details, the model can be used in a nested mode.

The values of Δx , Δy and $\Delta\theta$ are normally based on the above physical criteria but the value of Δx should additionally be based on a numerical stability criterion. For our model this criterion can be shown to be (by a Von Neumann stability analysis; e.g. Abbott, 1979):

$$\left| \frac{c_{0y}\Delta x}{c_{0x}\Delta y} \right| + \left| \frac{c_{0\theta}\Delta x}{c_{0x}\Delta\theta} \right| \leq 1 \quad (55)$$

In choosing the values of Δx , Δy and $\Delta\theta$ for a particular application of the HISWA model, we take the value of each of the terms on the left-hand side of Eq. 55 equal to or less than $1/2$. From this and the value of $\Delta\theta$, the values of Δx and Δy can be determined as shown below. The smallest of these values and the ones following from the above resolution considerations are to be used.

To estimate the grid size Δx , the ratio of the propagation velocities $c_{0\theta}$ and c_{0x} must be considered. It can be shown that in the absence of currents this ratio is maximal for long waves (phase velocity approximately equal to $(gd)^{1/2}$). Hence the second term on the left-hand side of Eq. 55 is always less than or equal to $1/2$ if (see Eq. 5):

$$\frac{\Delta x}{\Delta\theta} \leq \cos(\theta) \left[\frac{1}{d} \frac{\partial d}{\partial n} \right]^{-1} \quad (56)$$

Since in the HISWA model the maximum value of $|\theta|$ is typically 60° it follows from Eq. 56 that Δx and $\Delta\theta$ must be chosen such that (replacing the bottom slope normal to θ , $\partial d/\partial n$ by the bottom slope itself, $|Vd|$):

$$\frac{\Delta x}{\Delta \theta} \leq \frac{1}{2} \frac{d}{|\nabla d|} \quad (57)$$

To subsequently estimate the grid size Δy consider again a situation without currents. The direction θ is then equal to the direction of propagation so that:

$$\frac{c_{0y}}{c_{0x}} = \tan(\theta) \quad (58)$$

Using this expression one obtains a value of the first term on the left-hand side of Eq. 55 which is less than or equal to 1/2 if the ratio of Δx and Δy is chosen such that:

$$\frac{\Delta y}{\Delta x} \geq 2 \tan(\theta) \quad (59)$$

This implies that the maximum value of θ must be less than 90° so that the directional sector of wave propagation in the HISWA model is always less than 180° wide. In fact, the maximum value of θ is usually chosen to be 60° with $\Delta y/\Delta x$ equal to about 3.5.

For very shallow water criterion Eq. 57 often implies a fairly small value of Δx . Such a small value can be avoided if the numerical scheme is unconditionally stable. Work is therefore in progress to replace the upstream scheme for refraction with a fully implicit scheme. The present practice is to use a rather larger value of Δx (determined from the above spatial resolution requirements) and to restrict the refraction speed $c_{0\theta}$ when (occasionally) condition 55 is not met during the computations. Experience has shown that it does not occur very frequently and that it does not greatly affect the model results.

Integration scheme

The integration scheme in the model can be divided into two parts: the propagation of the waves on one hand and the generation and dissipation of the waves on the other. Both parts are briefly described below.

The computational grid (the wave-field grid) is a rectangular grid in (x,y,θ) -space (see Fig. 3) with its x -axis roughly parallel with the mean wave direction in the x,y -plane. The computations start at the upwave boundary at the plane $x=0$ in (x,y,θ) -space where the values of A_0 and ω_0 (and consequently also of c_{0x} , c_{0y} , and $c_{0\theta}$) are given for all locations along this boundary and for all spectral directions. The computations proceed step-wise in the x -direction. The values of A_0 and ω_0 for each (y,θ) -value in the plane $x=\Delta x$ in (x,y,θ) -space are computed from the wave information in the first plane ($x=0$). This process of propagation is repeated for each next step, that is, the values of A_0 and ω_0 in

the next plane, $x = (j + 1)\Delta x$ are determined solely from the wave information on the previous plane $x = j\Delta x$ (see Fig. 3).

The propagation in the model is carried out with the finite difference schemes mentioned in the section on Numerical method which have a first order accuracy in Δx , Δy and Δt if the option of added numerical diffusion is used.

The modelling of the growth and dissipation from the previous plane $x = j\Delta x$ to the next plane $x = (j + 1)\Delta x$ is partially explicit and partially implicit. The fairly smoothly behaving wind generation source terms are evaluated analytically in the model from only the previous wave information (at plane $x = j\Delta x$) to develop the waves from plane $x = j\Delta x$ to plane $x = (j + 1)\Delta x$. The other source terms are sometimes highly nonlinear, depending on the geophysical situation. To avoid unstable behaviour of these terms we have chosen an implicit representation of these terms, i.e. the evaluation of these terms in the model includes the (as yet unknown) wave information at the plane $x = (j + 1)\Delta x$. This implicit formulation can be combined with the explicit propagation in a simple manner, since it involves only one unknown value, i.e. $A_0(\theta)$.

Input/output

As indicated in the section on Boundary conditions, the model requires wave input at the up-wave boundary (either a discrete spectral representation of $E_0(\theta)$ and $\Omega_0(\theta)$ or a parametric representation, i.e. $E_0(\theta) = E_1 D_{\text{ideal}}(\theta)$). Additional input is limited to only the bottom topography and current field (on a regular grid), the wind speed and direction, grid definitions and output requests. Output of the primary results, $E_0(\theta)$ and $\omega_0(\theta)$ is available on grid points, or lines and locations which are all independent of the computational grid. Integral parameters such as the significant wave height:

$$H_s = 4 E_1^{1/2} \quad (60)$$

the mean wave period:

$$\bar{T} = 2 \pi \Omega_1^{-1} \quad (61)$$

and the mean wave direction θ and directional spreading σ_θ (following definitions used for the analysis of pitch-and-roll buoy wave data (e.g. Kuik et al., 1988):

$$\bar{\theta} = \arctan(b/a) \quad (62)$$

$$\sigma_\theta = [2\{1 - (a^2 + b^2)^{1/2}\}]^{1/2} \quad (63)$$

in which $a = \int_0^{2\pi} \cos(\theta) D(\theta) d\theta$ and $b = \int_0^{2\pi} \sin(\theta) D(\theta) d\theta$ and other secondary output such as the radiation stress gradient for short-crested waves (Battjes, 1972) are also available at the same output grid points, lines or locations.

TESTS

To assess the behaviour of the model as regards wave propagation, generation and dissipation the model has been successfully applied to rather basic idealized situations for which the results can be compared with analytical solutions or information in the literature (Booij et al., 1988). This is illustrated here for propagation towards a plane beach and in an opposing current. To compare the results with analytical solutions from linear wave theory the waves are taken as fairly long-crested ($\cos^{64}(\theta)$ -directional energy distribution) and all source terms have been set at zero (this implies that the mean frequency $\omega_0(\theta)$ remains constant). The waves approach a plane beach (slope 1:120) at an incidence angle in deep water of 30° . In the case of the opposing current (deep water) the waves approach a shear-current (current speed increasing cross-stream from 0 to 2 m s^{-1} over a distance of 1000 m) at an angle of incidence of 60° (30° off the normal to the current direction). The analytical solutions are based on conservation of action and wave number component in the direction normal to the beach or to the current. The results are given in Fig. 4 where it is obvious that the agreement between analytical solutions and numerical results is excellent. Wave growth in a standard situation is addressed in the section on Generation by wind (see Fig. 1).

Tests in laboratory conditions have been described by Booij et al. (1985) and Dingemans et al. (1987). Dingemans et al. (1987) have analyzed their tests quantitatively and in great detail. It concerned a situation with short-crested, random waves propagating around and across a submerged breakwater located in an otherwise flat area. The waves produced a relatively strong current caused by gradients in the wave-induced radiation stresses. These currents were measured and subsequently used as input to the HISWA model so that the test included wave-current interactions which were quite significant. An earlier version of the HISWA model was used which was slightly different from the model described here as regards some numerical and physical aspects. The observed rms-errors are typically about 5% in the significant wave height (H_s), 10–25% in mean period (\bar{T}) and about 5° in mean wave direction (% of observed values except directions). Considering the performance of conventional wave models in such situations these results are deemed to be satisfying. A more crucial test is of course the performance of the model in field conditions. The first test of the model under these conditions (no tuning of the model) is presented next.

To test the model in geophysical conditions which are more realistic and complicated than in the academic tests and laboratory tests indicated above, the model has been applied to an area of the Rhine estuary (the Haringvliet, see Fig. 5). This area was chosen because the model results can be compared with the results of a well documented field campaign of the Ministry of Transport and Public Works in the Netherlands (Dingemans, 1983, 1985; Dinge-

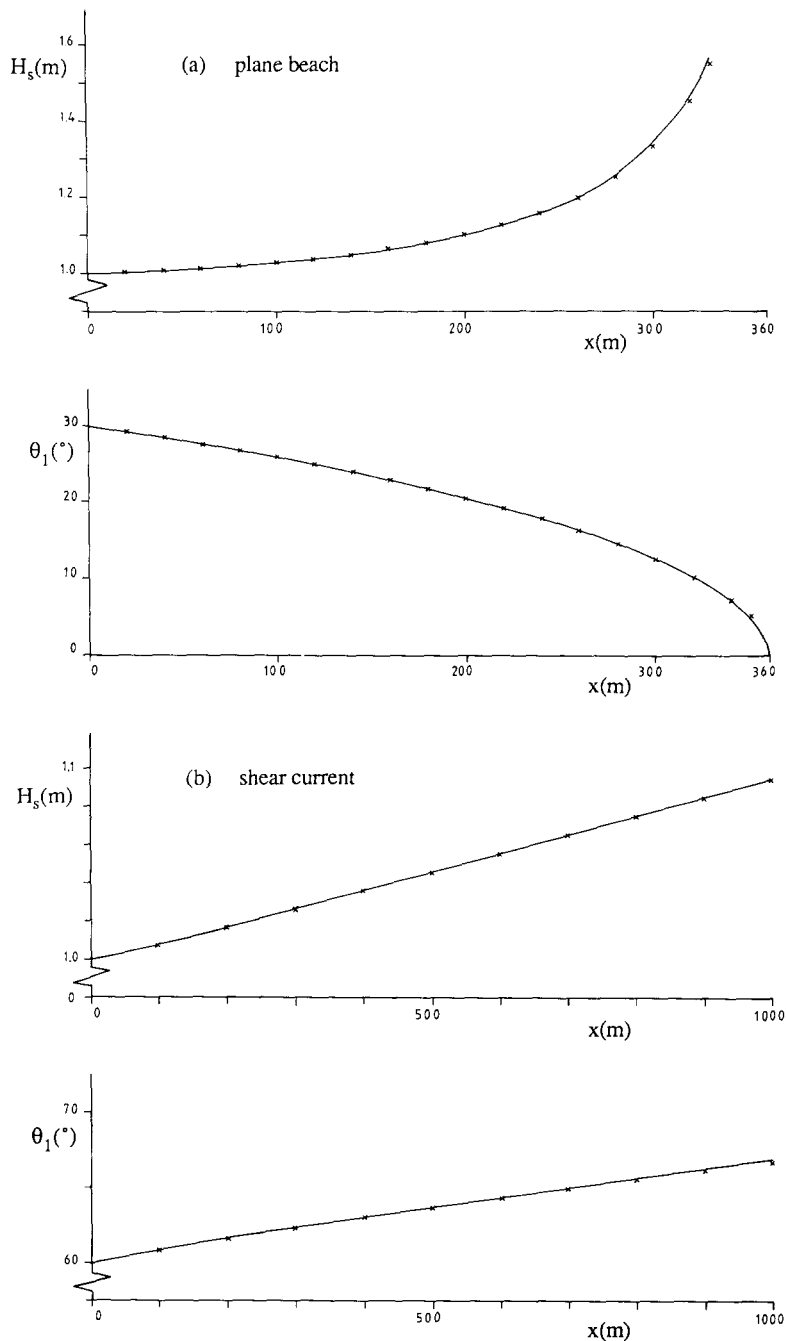


Fig. 4. Analytical solutions from linear wave theory (full lines) and numerical results from HISWA (crosses). Panel (a) for wave propagation towards a plane beach (angle of incidence 30°). Panel (b) for propagation through a shear current (angle of incidence 60° , current speed increasing linearly from 0 to 2 m/s over 1000 m). The waves are fairly long-crested ($\cos^{6.4}(\theta)$ -directional energy distribution) and their (mean) wave period is 5 s.

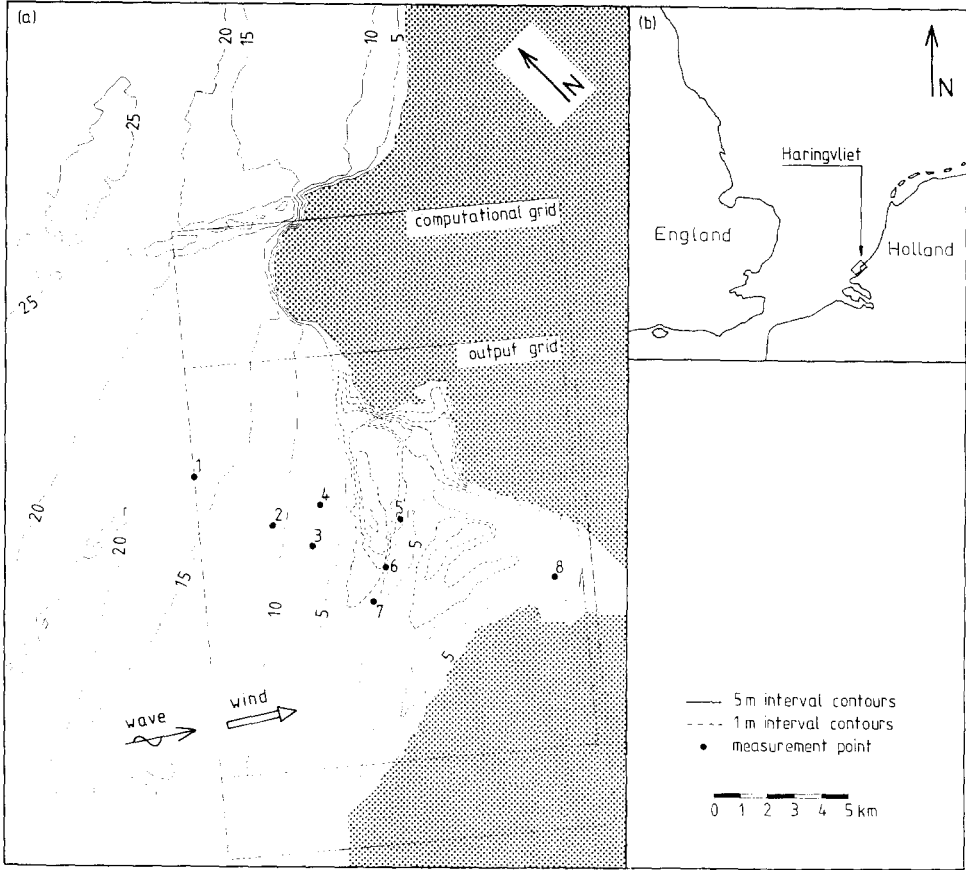


Fig. 5. Location and bathymetry of the Haringvliet estuary and locations of the WAVEC buoy (1), the waverider buoys (2-7) and the wave gauge (8).

mans et al., 1985). This campaign involved the use of one WAVEC pitch-and-roll buoy, one wave gauge and six waverider buoys. The situation can be characterized as non-locally generated waves passing from deeper water into shallow water over a shoal with a regeneration by wind behind the shoal. Currents are practically non-existent in the chosen situation because this particular branch of the Rhine estuary is closed by gates. The location and bathymetry of the study area are indicated in Fig. 5 with the locations of the buoys and the wave gauge. The bathymetry can be roughly characterized as a relatively shallow river mouth, no currents, water depth typically 4-5 m, about 10×10 km in surface area. It is partly protected from the southern North Sea by a shoal of roughly 2×4 km (water depth typically 1-2 m) extending over half the mouth opening.

The computations have been carried out for a situation which occurred on October 14, 1982 at 22.00 h (M.E.T.). The waves are locally generated in the

southern North Sea with a significant wave height of about 3 m and a mean period of about 7 s at the estuary entrance (location 1, Fig. 5). These waves penetrate the area from a northwesterly direction. They break over the shoal with a reduction in wave height from about 2.5 to about 0.5 m over the shoal. The local wind of 16.5 m s^{-1} from a northwesterly direction regenerates the waves to about 0.9 m significant wave height at the wave gauge which is located 5 km behind the shoal (location 8, Fig. 5). Quantitative information is provided in Table 1 (after Dingemans, 1983, 1985). The WAVEC pitch-and-roll buoy in 16 m water depth (location 1, Fig. 5) provides the significant wave height, the peak wave period (the inverse of the peak frequency of the energy spectrum), the mean wave direction and the directional width as input at the up-wave boundary of the model (for parameter values see Table 1). We assume a $\cos^2(\theta)$ -directional frequency-integrated energy distribution, commensurate with the directional spreading of $\sigma_\theta = 31^\circ$ as observed by the WAVEC buoy. The waverider buoys and the wave gauge are located at various positions in the area (locations 2–7, Fig. 5) each providing a significant wave height and a mean wave period which can be compared to the results of the model.

The pattern of the model results, shown in Figs. 6 (panel a) and 7 and indicated as “standard” in Table 1, is consistent with the pattern of the observations, e.g. the significant wave height which at the up-wave boundary of the model (16 m water depth) is about 3.4 m, reduces gradually to about 2.5 m at 6 m depth and then very rapidly to about 0.6 m over the shoal. South of the shoal the gradual shoreward decrease in wave height continues. At the location of the wave gauge (about 5 km behind the shoal; location 8 in Fig. 5) the sig-

TABLE 1

Observations and model results at various locations in the Haringvliet of the significant wave height H_s and the mean wave period \bar{T}

location	instrument	measurement		HISWA					
		H_s (m)	\bar{T} (s)	standard		no refraction		no wind	
				H_s (m)	\bar{T} (s)	H_s (m)	\bar{T} (s)	H_s (m)	\bar{T} (s)
1	wavec	3.38	7.0*	—	—	—	—	—	—
2	waverider	2.90	6.3	3.27	6.8	3.31	6.8	3.25	6.8
3	waverider	2.58	6.3	2.62	5.9	2.61	5.8	2.62	5.9
4	waverider	2.68	5.9	2.56	5.8	2.54	5.7	2.56	5.8
5	waverider	0.62	2.6	0.68	2.8	0.65	2.9	0.60	2.8
6	waverider	1.05	3.7	1.01	3.4	1.03	3.4	0.76	3.2
7	waverider	1.60	5.1	1.37	3.8	1.36	3.8	1.35	3.7
8	wave gauge	0.95	2.8	0.83	3.4	0.94	3.5	0.64	3.2

*taken as $0.85 T_p$ where T_p is the observed peak period of 8.3 s.

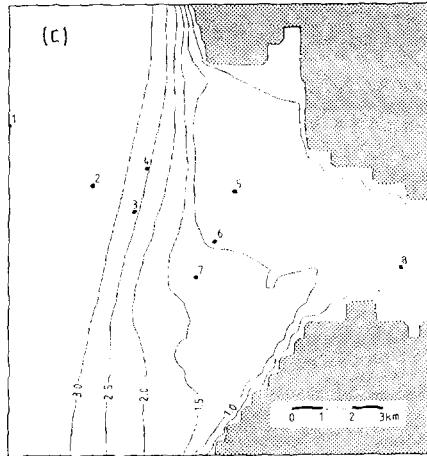
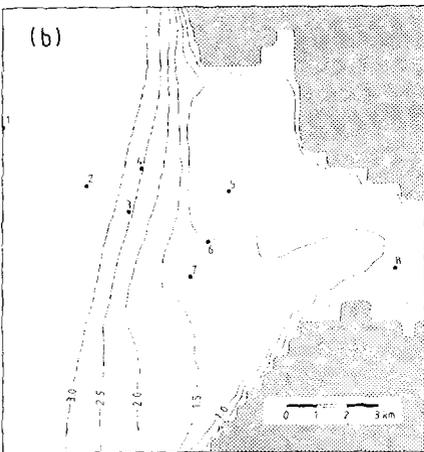
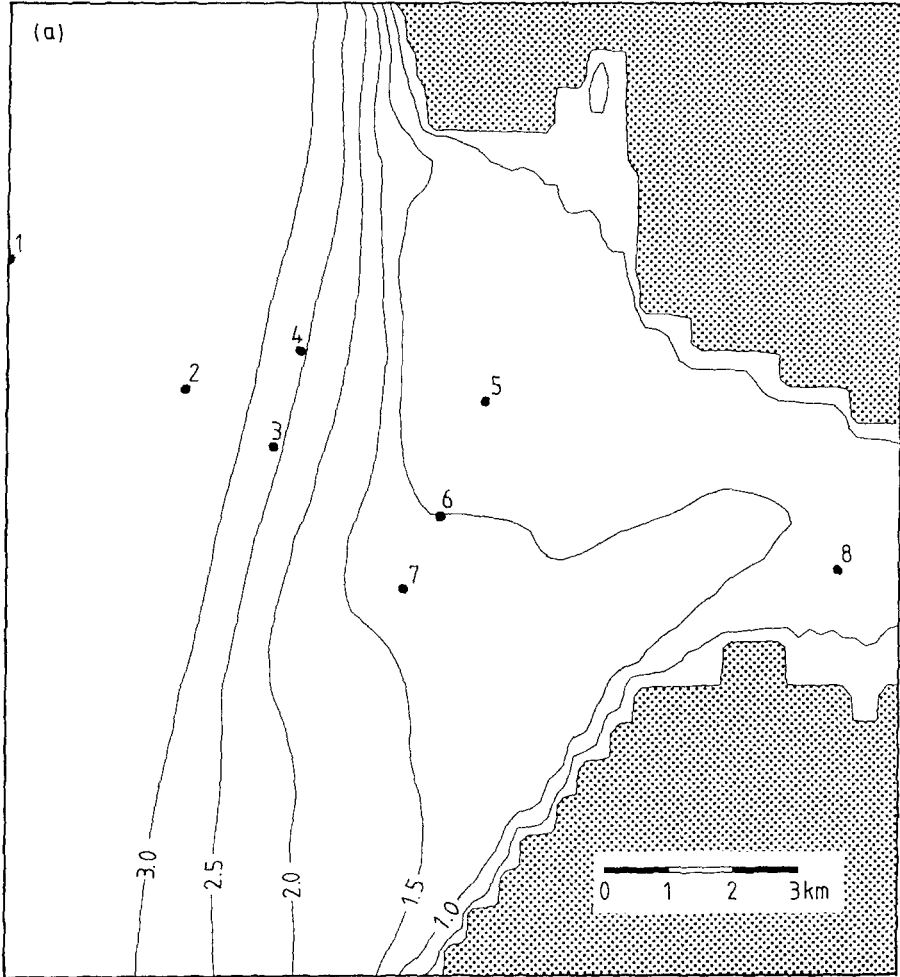


Fig. 6. Contour line plot of significant wave height, contour line interval 0.5 m. Panel (a) standard computations; panel (b) computations without refraction; panel (c) computations without wind.



Fig. 7. Contour line plot of mean wave period, contour line interval 1 s (standard computation).

nificant wave height is about 0.8 m. The mean wave period follows roughly the same pattern (Fig. 7).

The initial gradual decrease of wave height is caused by bottom dissipation whereas the rapid decrease near the shoal is caused by wave breaking. The effect of refraction is relatively unimportant as illustrated with the results of a computation in which the refraction term has been set at zero (see Fig. 6, panel b and Table 1). This minor influence of refraction on the spatial wave height distribution is a result of the short-crestedness of the waves. The focussing and defocussing of individual directional components tend to cancel in a short-crested sea. Such short-crestedness can in principle also be properly accounted for in models based on the wave-ray technique (although it would be uneconomical to add wave generation and dissipation, see Introduction) but only in a discrete spectral manner. In the conventional monochromatic, unidirectional wave-ray approach unrealistic results are obtained in this case, in particular behind the shoal (see Fig. 8; with the same (mean) wave period and (mean) wave direction at the upwave boundary). Behind the shoal the waves are regenerated by the wind. This is illustrated by applying the model to the same situation (including refraction) but without wind (Fig. 6, panel c and Table 1).

The differences (rms-errors) between the observations and the model results (labelled "standard" in Table 1, i.e. computations including refraction and wind generation) are 0.18 m and 0.6 s for the significant wave height and the mean wave period respectively. This is 10.2 and 13.0% respectively of the

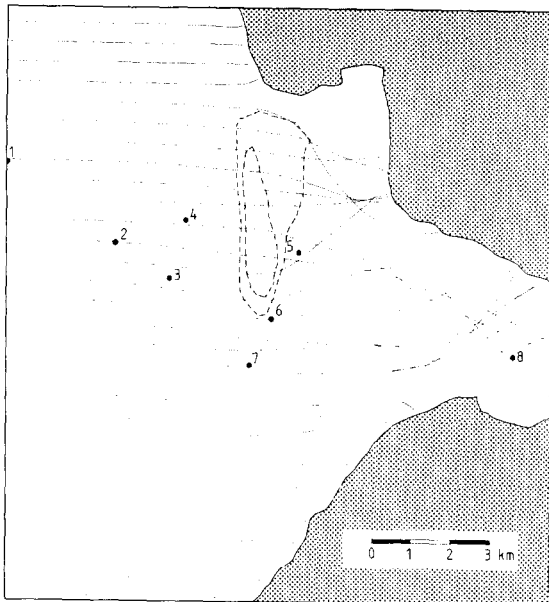


Fig. 8. Wave rays for 7 s period monochromatic, unidirectional waves.

mean observed values. The mean errors for the significant wave height and mean period are small (less than 0.01 m and 0.1 s respectively).

The above rms-errors are partly based on data from locations near the upwave boundary where any reasonable model will produce small errors since little happens to the waves anyway. On the other hand, some data are from locations where the waves have been modified considerably (e.g. a factor five in significant wave height at location 5). A good model should reproduce such large changes. Such a quality however is not properly expressed by rms-errors. For instance, the field tests of the model of Resio (1987, 1988) show a small rms-error in the significant wave height (0.16 m which is only 7.1% of the observed mean value) but the observed change in significant wave height is also small (0.41 m rms-value). A more suitable measure for the model performance, in which the boundary situation cannot dominate, is therefore defined as the performance of a perfect model (unity) minus the performance of the model relative to the observed changes (from the upwave boundary):

$$\text{performance rate} = 1 - \frac{\text{rms (error)}}{\text{rms (observed changes)}} \quad (64)$$

For the above tests with the HISWA model the rms-value of the changes in significant wave height is 1.83 m and in mean wave period 2.4 s. With the above rms-errors, the performance rates for the HISWA model are then 0.91 and 0.76

respectively for the significant wave height and the mean wave period. This compares favourably with 0.61 for the significant wave height in the field tests of the model of Resio (1987, 1988; model wave periods not available).

CONCLUSIONS

The wave prediction model HISWA presented here is a stationary, directionally decoupled parametric model for predicting short-crested waves in shallow water with arbitrary bottom topography and current patterns. The phenomena accounted for are shoaling, refraction, wind generation, wave breaking (surfzone inclusive), bottom dissipation and wave blocking including the influence of currents on these phenomena. The basis of the model is the prediction of two directional wave functions: the one-dimensional directional action spectrum and the average frequency as a function of spectral direction. From these functions (in each of a large number of grid points in the geographical prediction area), the model determines integral functions such as the significant wave height, the average wave period and the mean wave direction and other functions such as the radiation stress gradient. For reasons of computing efficiency the computations are carried out on a regular grid rather than along wave rays.

The model is stationary, i.e. the environment (depth, wind and current) is not allowed to vary in time and the predicted wave functions are also constant in time. This is normally not a serious restriction for wave computations in coastal regions because the travel time of the waves in such regions is usually small compared to the time scales of variations in depth, wind and currents. If such slow variations are to be taken into account then the wave model should be applied in a sequence of stationary situations which approximate the non-stationary situation.

After passing a number of academic tests the model has been applied to a fairly complex situation in the mouth of the river Rhine in which wave breaking and short-crestedness dominate other effects such as refraction. The rms-errors for the significant wave height and the mean wave period for this situation are about 10 and 13% of the mean observed values respectively. This implies that in this situation HISWA correctly reproduces about 90% of the observed changes in the significant wave height and about 75% of the observed changes in the mean wave period.

ACKNOWLEDGEMENTS

The HISWA model has been developed under contract with the Department of Transport and Public Works in the Netherlands. We greatly appreciate the support of and discussions with our colleagues A.J. Kuik and J.A. Vogel of this Department and with M.W. Dingemans of Delft Hydraulics. We thank J.A.

Battjes of the Delft University of Technology for his comments on early drafts of this paper and J. Dekker for assisting us in the computations.

REFERENCES

- Abbott, M.B., 1979. *Computational Hydraulics*. Pitman, London, 324 pp.
- Arthur, R.S., Munk, W.H. and Isaacs, J.D., 1952. The direct construction of wave rays. *Trans. Am. Geoph. Union*, 33: 855-865.
- Barnett, T.P., 1968. On the generation, dissipation and prediction of ocean wind waves. *J. Geophys. Res.*, 73: 513-534.
- Battjes, J.A., 1968. Refraction of water waves. *ASCE J. Waterw. Harbors Div.*, 94, WW4 (Nov.): 437-451.
- Battjes, J.A., 1972. Radiation stresses in short-crested waves. *J. Mar. Res.*, 30: 56-64.
- Battjes, J.A. and Janssen, J.P.F.M., 1979. Energy loss and set-up due to breaking of random waves. In: *Proc. 16th Int. Coastal Engineering Conference, 1978, Hamburg*. ASCE, New York, N.Y., pp. 569-587.
- Booij, N., Holthuijsen, L.H. and Herbers, T.H.C., 1985. A numerical model for wave boundary conditions in port design. In: J.H. Pounsford (Editors), *Proc. Int. Conf. Numerical and Hydraulic Modelling of Ports and Harbours*, Birmingham, pp. 263-268.
- Booij, N., Holthuijsen, L.H., Dekker, J. and Schoonbeek, R., 1988. Standard tests for the shallow water wave model HISWA. *Delft Univ. Technol., Dep. Civ. Eng., Group Hydraul. Geotech. Eng.*, Rep. No. 6-88, 42 pp.
- Bouws, E., Günther, H., Rosenthal, W. and Vincent, C.L., 1985. Similarity of the wind wave spectrum in finite depth water: 1. Spectral form. *J. Geophys. Res.*, 90: 975-986.
- Bretherton, F.P. and Garrett, G.J.R., 1968. Wavetrains in inhomogeneous moving media. *Proc. R. Soc. London*, A302: 529-554.
- Brink-Kjær, O., 1984. Depth-current refraction of wave spectra. In: *Proc. Symp. Description and Modelling of Directional Seas, 1984, Copenhagen*. Pap. C-7. Tech. Univ. Denmark, Copenhagen, 12 pp.
- Cavaleri, L. and Malanotte Rizzoli, P., 1981. Wind wave prediction in shallow water: theory and applications. *J. Geophys. Res.*, 86: 10961-10973.
- CERC, 1973. *Shore Protection Manual*. U.S. Army Coastal Eng. Res. Center, Corps Engineers. 1145 pp.
- Chen, Y. and Wang, H., 1983. Numerical model for nonstationary shallow water wave spectral transformations. *J. Geophys. Res.*, 88: 9851-9863.
- Collins, J.I., 1972. Prediction of shallow water spectra. *J. Geophys. Res.*, 77: 2693-2707.
- Dingemans, M.W., 1983. Verification of numerical wave equation models with field measurements, CREDIZ verification Haringvliet. *Delft Hydraulics Lab.*, Rep. No. W488, Delft, 137 pp.
- Dingemans, M.W., 1985. Surface wave propagation over an uneven bottom, Evaluation of two-dimensional horizontal wave propagation models. *Delft Hydraulics Lab.*, Rep. No. W301, part 5, Delft, 117 pp.
- Dingemans, M.W., Stive, M.J.F., Kuik, A.J., Radder, A.C. and Booij, N., 1985. Field and laboratory verification of the wave propagation model CREDIZ. In: B.L. Edge (Editor), *Proc. 19th Int. Coastal Eng. Conf.*, 1984, Houston. ASCE, New York, N.Y., pp. 1178-1191.
- Dingemans, M.W., Stive, M.J.F., Bosma, J., De Vriend, H.J. and Vogel, J.A., 1987. Directional nearshore wave propagation and induced currents. In: B.L. Edge (Editor), *Proc. 20th Int. Coastal Eng. Conf.* (Nov. 1986), Taipei. ASCE, New York, N.Y., pp. 1092-1106.
- Donelan, M.A., Hamilton, J. and Hui, W.H., 1985. Directional spectra of wind-generated waves. *Philos. Trans. R. Soc. London*, A315: 509-562.

- Ewing, J.A., 1971. A numerical wave prediction method for the North Atlantic Ocean. *Dtsch. Hydrogr. Z.*, 24: 241-261.
- Gelci, R., Cazale, H. and Vassal, J., 1956. Utilisation des diagrammes de propagation à la prévision énergétique de la houle. *Bulletin d'information du Comité central d'océanographie et d'études des côtes*, 8: 169-197.
- Golding, B., 1983. A wave prediction system for real-time sea state forecasting. *Q. J. Met. Soc.*, 109: 393-416.
- Graber, H.C. and Madsen, O.S., 1985. A parametric wind wave model for arbitrary water depths. In: Y. Toba and H. Mitsuyasu (Editors), *The Ocean Surface*. D. Reidel, Dordrecht, pp. 193-199.
- Günther, H., 1981. A parametric surface wave model and the statistics of the prediction parameters. Ph.D. thesis. *Hamburger Geophysikalische Einzelschriften*, A55, 90 pp.
- Günther, H., Rosenthal, W. and Richter, K., 1979. A hybrid parametrical wave prediction model. *J. Geophys. Res.*, 84: 5727-5738.
- Hasselmann, K., 1960. Grundgleichungen der Seegangsvoraussage. *Schiffstechnik*, Vol. 7, No. 39: 191-195.
- Hasselmann, S. and Hasselmann, K., 1981. A symmetrical method of computing the nonlinear transfer in a gravity wave spectrum. *Hamburger Geophysikalische Einzelschriften*, Max-Planck-Institut für Meteorologie, A52, 177 pp.
- Hasselmann, K., Barnett, T.P., Bouws, E., Carlson, H., Cartwright, D.E., Enke, K., Ewing, J.A., Gienapp, H., Hasselmann, D.E., Kruseman, P., Meerburg, A., Müller, P., Olbers, D.J., Richter, K., Sell, W. and Walden, H., 1973. Measurements of wind-wave growth and swell decay during the Joint North Sea Wave Project (JONSWAP). *Dtsch. Hydrogr. Z.*, A8, No. 12, 95 pp.
- Hasselmann, K., Ross, D.B., Müller, P. and Sell, W., 1976. A parametric wave prediction model. *J. Phys. Oceanogr.*, 6: 200-228.
- Hasselmann, S., Hasselmann, K., Allender, J.H. and Barnett, T.P., 1985. Computations and parameterizations of the nonlinear energy transfer in a gravity-wave spectrum. Part II: Parameterizations of the nonlinear energy transfer for applications in wave models. *J. Phys. Oceanogr.*, 15: 1378-1391.
- Hirosue, F. and Sakai, T., 1987. Directional spectra in current-depth refraction. In: B.L. Edge (Editor), *Proc. 20th Int. Coastal Eng. Conf. (Nov. 1986)*, Taipei. ASCE, New York, N.Y., pp. 247-260.
- Holthuijsen, L.H., 1983. Observations of the directional distribution of ocean-wave energy in fetch-limited conditions. *J. Phys. Oceanogr.*, 13: 191-207.
- Janssen, P.A.E.M., Komen, G.J. and De Voogt, W.J.P., 1984. An operational coupled hybrid wave prediction model. *J. Geophys. Res.*, 89: 3635-3654.
- Karlson, T., 1969. Refraction of continuous ocean wave spectra. *Proc. ASCE J. Waterw. Harbors Div.*, Vol. 95, No. WW4: 437-448.
- Kitaigorodskii, S.A., Krasitskii, V.O. and Zaslavskii, M.M., 1975. On Phillips' theory of equilibrium range in the spectra of wind-generated gravity waves. *J. Phys. Oceanogr.*, 5: 410-420.
- Kuik, A.J., Van Vledder, G.Ph. and Holthuijsen, L.H., 1988. A method for the routine analysis of pitch and roll buoy wave data. *J. Phys. Oceanogr.*, 18: 1020-1034.
- Mathiesen, M., 1984. Current-depth refraction of directional wave spectra. In: *Symp. Description and Modelling of Directional Seas, 1984*, Copenhagen. Pap. No. C-6. Tech. Univ. Denmark, Copenhagen, 8 pp.
- Miche, R., 1944. Mouvements ondulatoires de la mer en profondeur constante ou décroissante. *Ann. Ponts Chaussées*, 114: 369-406.
- Phillips, O.M., 1977. *The dynamics of the Upper Ocean*. Cambridge University Press, 336 pp.
- Pierson, W.J. and Moskowitz, L., 1964. A proposed spectral form for fully developed wind seas based on the similarity theory of S.A. Kitaigorodskii. *J. Geophys. Res.*, 69: 5181-5190.
- Piest, J., 1965. Seegangsbestimmung und Seegangsrefraktion in einem Meer mit nicht-ebenem Boden - eine theoretische Untersuchung. *Dtsch. Hydrogr. Z.*, 18: 67-74.

- Putnam, J.A. and Johnson, J.W., 1949. The dissipation of wave energy by bottom friction. *Trans. Am. Geoph. Union*, 30: 67-74.
- Resio, D.T., 1987. Shallow-water waves. I: Theory. *Proc. ASCE J. Waterw., Ports Coastal Ocean Eng.*, 113: 264-281.
- Resio, D.T., 1988. Shallow-water waves II: Data comparisons. *Proc. ASCE J. Waterw., Ports Coastal Ocean Eng.*, 114: 50-65.
- Sakai, T., Kosecki, M. and Iwagaki, Y., 1983. Irregular wave refraction due to current. *J. Hydraul. Eng., ASCE*, 109: 1203-1215.
- Seymour, R.J., 1977. Estimating wave generation on restricted fetches. *Proc. ASCE, J. Waterw., Port Coastal Ocean Div.*, 103, No. WW2: 251-264.
- Thornton, E.B., 1977. Rederivation of the saturation range in the frequency spectrum of wind-generated gravity waves. *J. Phys. Oceanogr.*, 7: 137-140.
- Whitham, G.B., 1965. A general approach to linear and nonlinear dispersive waves using a Lagrangian. *J. Fluid Mech.*, 22: 273-284.
- Whitham, G.B., 1971. Dispersive waves and variational principles. In: A.H. Tahb (Editor), *Studies of Applied Mathematics*, 7: 181-212.
- Young, I.R., 1988. A shallow water spectral wave model. *J. Geophys. Res.*, 93: 5113-5129.